Journal of Non-Crystalline Solids 387 (2014) 117–123

Contents lists available at ScienceDirect

Journal of Non-Crystalline Solids

journal homepage: www.elsevier.com/ locate/ jnoncrysol

The effects of Si substitution on the glass forming ability of Ni–Pd–P system, a DFT study on crystalline related clusters

J.A. Reyes-Retana *, G.G. Naumis

Departamento de Física-Química, Instituto de Física, Universidad Nacional Autónoma de México (UNAM), Apartado Postal 20-364, 01000 Mexico, Distrito Federal, Mexico

ARTICLE INFO

Article history:
Received 3 December 2013
Received in revised form 30 December 2013
Available online xxxx

Keywords:
Metallic Glasses;
Glass Formation;
Electronic Structure

ABSTRACT

In order to investigate the influence of Si in the glass forming ability of Pd–Ni–P based bulk metallic glasses, the topological and electronic structure of stoichiometry related crystals is explored using density functional theory. The results indicate that Si based clusters based on a rich Pd environment with a symmetric configuration of the transition metal are the most stable, while P prefers a Ni rich environment with an asymmetric arrangement of the transition metals. Si tends to be at the center of the clusters, while in general the P atoms present a displacement toward some of the Ni atoms. The coordination of Si in rich Ni crystals is always higher than the one observed for P atoms. Also, the inclusion of Si induces a local pressure field in a radius of 14 Å leading to a disordered displacement of P from the equilibrium positions. The favoring of different competing crystals by adding Si, as well as the local pressure effect, suggests a mechanism on how devitrification is suppressed.

1. Introduction

The metallic amorphous alloys have been attracting much attention due to their unusual properties comparing with their crystalline phases. Such potential properties are, for example, corrosion resistance, temperature-insensitive electrical conductivity, ductility, and high strength [1]. Nowadays there are several bulk metallic glass (BMG) systems, although it is not clear so far the physical origin of this glass formation [2]. The history of BMG started with the $Au_{75}Si_{25}$ alloy, that was first reported by Klement et al. in 1960 [3]. Then Pd-based metallic alloys were made by rapid melt quenching. With this method, Chen prepared millimeter-diameter rods of Pd–Cu–Si BMG [4]. Using the Pd-based BMG, Drehman et al. prepared the famous Pd–Ni–P BMG [5,6]. They used boron oxide fluxing method to prevent heterogeneous nucleation. One fact that limits the Pd-based BMG mass production is the high cost of the Pd metal, therefore it was necessary to search new metal-based BMG compositions. Inoue and coworkers had found new multicomponent BMGs with excellent glass-formation ability (GFA) [7], for example: Mg-, Ln–Zr-, Fe-, Pd–Cu-, Pd–Fe-, Ti- and Ni-based alloy systems. In this context, $Pd_{40}Ni_{10}Cu_{Cu}P_{20}$ and $Pd_{42.5}Ni_{7.5}Cu_{30}P_{20}$ have the lowest critical cooling rate of 0.10 and 0.067 K/s, which can be associated to the best GFA [8,9].

Several criteria for determining GFA have been proposed, for example, the reduced glass transition temperature T_{rg}, proposed by Turnbull [10], which corresponds to the ratio of the glass transition temperature (T_g) to the melting point (T_m) of alloy. Also, the criteria $1/(T_g + T_l)$ and T_x can be used, where T_g, T_l and T_x are the glass transition, the liquidus and the onset crystallization temperatures, respectively [11]. Experimentally, one factor that spoils the glass-formation abilities is the small oxide particles within the melt, this limitation can be improved by fluxing B_2O_3 [6]. The crystallization in $Pd_{40}Ni_{40}P_{20}$ can be either from internal nuclei or from surface impurities, therefore heterogeneous nucleation is an important limitation on the GFA [12–14].

It was reported that, with a minor addition of Si, Pd–Ni–P and Cu–Hf–Ti BMGs had significantly improved of the GFA [15–17]. In the cases of $Pd_{40}Ni_{40}P_{20}$ and $Pd_{20}Ni_{60}P_{20}$ systems, it is not clear why only with the small addition of Si (4% and 2%), $\Delta T_x = T_x - T_g$ reached a maximum (120 and 74 K). Zeng et al. pointed out that with this percent, the heterogeneous crystallization was suppressed. It is important to remark that with a higher Si content the GFA is decreased.

In this work, we discuss the influence of the trigonal prism cluster units with P occupying the center site. Also, we focus on the substitution of P by Si in Pd–Ni–P systems. To do this, we studied several related crystalline phases in which is known that the same clusters observed in the glass appear [18].

Our main results indicate that Si tends to promote completing crystals favoring the formation of glass. Also, Si produces a kind of shoving effect by inducing a local internal pressure field in a radius of 14 Å which interferes with the off-center P displacement inside clusters. The different connectivity of the network can help to explain the improved mechanical properties as explained by J.C. Phillips rigidity theory [19–26].

The layout of this work is the following. We start with the description of the Pd–Ni–P and Pd–Ni–Si crystals and methods used. Then the structural effects of the Si inclusion are analyzed, which are followed by the study of the electronic properties. Finally, the conclusions are given.

* Corresponding author. Tel.: +52 55 5622 5174.
E-mail address: angelreyes@fisica.unam.mx (J.A. Reyes-Retana).

0022-3093/$ – see front matter © 2013 Elsevier B.V. All rights reserved.
http://dx.doi.org/10.1016/j.jnoncrysol.2014.01.001

Table 1
Crystallographic details of the Ni–P, Pd–Ni–P, Pd–P and Pd–Ni–Si systems [27,28].

Empirical formula	Space group	a (Å)	b (Å)	c (Å)
Ni_2P	$P\bar{6}2m$	5.87	5.87	3.39
PdNiP	$P\bar{6}2m$	6.02	6.02	3.60
Pd_3 P	Pnma	5.70	7.54	5.12
$PdNi_2P$	Cmcm	3.47	8.44	6.61
PdNiSi	$P\bar{6}2m$	6.27	6.27	3.35

2. Materials and methods

We have decided to focus on the Pd–Ni–P systems by studying the related crystalline structures: Ni_2P, PdNiP, $PdNi_2P$, Pd_3P and by systematically replacing P by Si in several compounds. Also, the PdNiSi and $PdNi_2$ Si crystals were studied. The corresponding crystallographic structures were obtained from references [27,28] and detailed in Table 1. All the corresponding structures were relaxed using usual atomic simulation techniques based on density functional theory (DFT).

These ab initio calculations were done by using the Quantum ESPRESSO [29] plane wave DFT and density functional perturbation theory (DFPT) code, available under the GNU Public License [30].

Scalar relativistic and non-spin polarized calculation were performed. A plane-wave basis set with the cutoff of 612 eV was used. Also, an ultrasoft pseudo-potential [31] from the standard distribution generated using a modified RRKJ [32] approach, and the generalized gradient approximation [33] (GGA) for the exchange-correlation functional in its PBE parametrization [34] was used. All atomic positions and lattice parameters of the supercells were optimized using the conjugate gradient method. The convergence for energy was chosen as 10^{-7} eV between two consecutive steps and the maximum forces acting are smaller than 0.05 eV/Å. The stress in the periodic direction is lower than 0.01 GPa in all cases.

Of special importance is the $PdNi_2P$ crystal, which is the closest one to the $Pd_{20}Ni_{60}P_{20}$ experimentally studied glass [16]. The $PdNi_2P$ primitive cell is trigonal with $a = 4.8761$ Å and $c = 6.6081$ Å ($\rho = 8.74$ gr/cm^3) [28]. This primitive cell was grown from 8 atoms to supercells of 16, 32, 64 and 128 atoms.

As the supercell grows, the % Si concentration can be decreased in order to achieve the goal of a small P substitution. Si was put in the following concentrations: $Pd_2Ni_4(P_1Si_1)$ (25% Si), $Pd_4Ni_8(P_3Si_1)$ (6.25% Si), $Pd_8Ni_{16}(P_8Si_1)$ (3.13% Si), $Pd_{16}Ni_{32}(P_{15}Si_1)$ (1.6% Si), and $Pd_{32}Ni_{64}(P_{31}Si_1)$ (0.8% Si). The corresponding structural and electronic properties are described in the following sections.

3. Results and discussion

3.1. Structural properties

The basic building block of Pd–Ni–P systems is based on trigonal prisms, with a P at the center of the prisms [7,18]. Six transition metals (TM) are in the corners of the prisms while three other TM are in the faces, as detailed in Fig. 1.

Several interesting features were obtained after the system relaxation,

1) Observations in pure Pd–Ni–P systems
As the basic crystal PdNiP is enriched with Ni, the relaxation of Pd–Ni–P systems shows that P tends to move slightly away from the center of the trigonal prisms, see Fig. 2. The reason is that in PdNiP, there are three Pd in the faces of the trigonal prism, as indicated in Fig. 1. However, as Ni replaces Pd, the TM are not placed

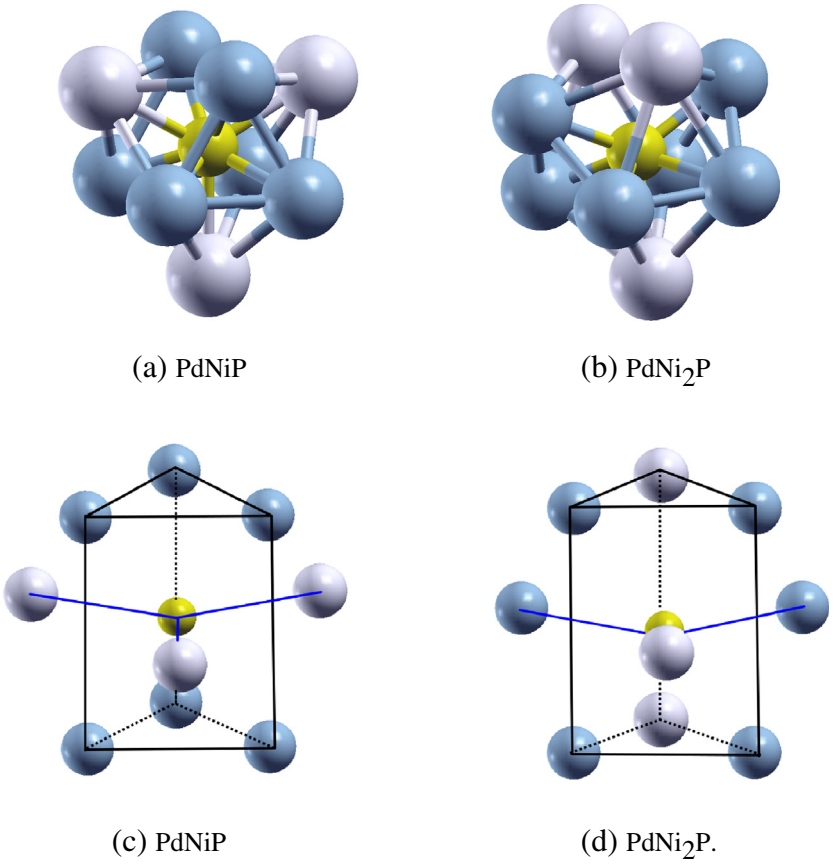

Fig. 1. The building blocks of PdNiP (1-a and 1-c) and $PdNi_2P$ (1-b and 1-d) with different ball sizes and orientations. Notice in (d) the small displacement of the P atom from the center of the trigonal prism in $PdNi_2P$, and how this results in two P– Pd broken bonds in (b). Gray, blue and yellow balls represent palladium, nickel and phosphorus, respectively. (For interpretation of the references to color in this figure legend, the reader is referred to the web version of this article.)

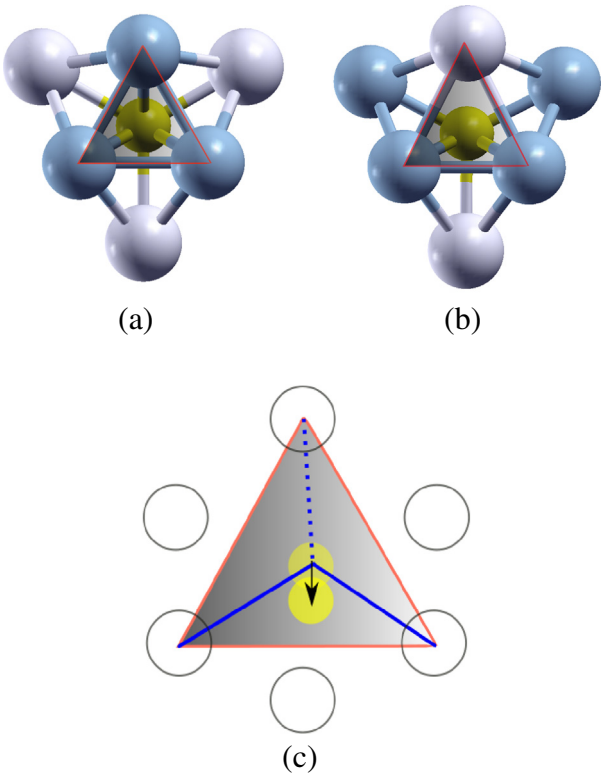

Fig. 2. Central P viewed from the top of the trigonal prism in 2-a PdNiP and 2-b $PdNi_2P$. In inset 2-c, we present a schematic cut of the prism. The dashed line corresponds to a P – Pd broken bond, while the arrow indicates the movement performed by the P atom from the center as Ni is added. The same color code of Fig. 1 is used. (For interpretation of the references to color in this figure legend, the reader is referred to the web version of this article.)

symmetrically in the plane that cuts the trigonal prism at the middle. As a result, P tends to stick with the Ni, and the two distances from Pd increase from 2.43 to 2.54 Å and one decreases from 2.43 to 2.41 Å, bringing as a consequence two broken P – Pd bonds and one stronger P – Pd bonds, respectively. The local structure of the P centered cluster and the corresponding distances between atoms are detailed in Fig. 1 and Table 2. A good agreement is found with the experimental observed values. The movement of the central P is correlated with changes in the electronic structure, as will be discussed later on.

We have tested several pressures in order to study the effects upon the central P movement in $PdNi_2P$. By applying 100 K bars, P returns to the center of the clusters.

2) Inclusion of Si on Pd–Ni–P

Contrasting with the previous behavior, when P is gradually replaced by Si at the center of the clusters, the local environment around Si is almost the same for all compositions, preserving all the bonds as seen in Fig. 3. As a consequence, the coordination of Si is *always the same as* P in the crystal PdNiP. Thus, this is a clear indication that Si tends to stabilize the clusters based on the trigonal prism even for an asymmetric distribution of TM. Also, Si has another important effect on the surrounding P based clusters. Since Si is bigger than P, the edges of the trigonal prism are increased as indicated in Table 2. We have found that this induces a local internal pressure that tends to move neighboring P atoms from its equilibrium value. This behavior is a kind of shoving [35,36], where the local cluster expansion around Si leads to a domino effect that propagates along the system. One can speculate that this helps to increase the GFA with only a 1% or 2% of Si.

Table 2
Distances inside the building block for PdNiP, $PdNi_2P$, PdNiSi and $PdNi_2Si$ as obtained from DFT. The values in parentheses are the experimental values [27,28].

System PdNiP distances		$PdNi_2P$ distances
P–Ni	2.38 (2.37) Å	2.24 (2.26) and 2.28 (2.29) Å
P–Pd	2.43 (2.45) Å	2.41 (2.42) and 2.54 (2.50) Å
Pd–Ni	2.80 (2.80) Å	2.76 (2.76) and 2.84 (2.85) Å
System PdNiSi distances		**$PdNi_2Si$ distances**
Si–Ni	2.35 (2.32) Å	2.31 and 2.32 Å
Si–Pd	2.46 (2.54) Å	2.44 and 2.49 Å
Pd–Ni	2.78 (2.78) Å	2.77 and 2.81 Å

To test the previous hypothesis, one can extract from the simulations the characteristic length of the Si influence. Thus, we calculated the ratios between the distances from P to each kind of non-equivalent TM as a function of the P atom distance from the Si. This allows to detect which bonds tend to be broken as the P moves from the center of the cluster as a function of the distance from the Si. Two kinds of ratios are defined. If we define d^f_{TM} as the distance from P to the TM on the faces and $d^t{}_{PTM}$ as the distance from P to the corners of the prisms, then the ratio d^f_{P-Ni}/d^f_{P-Pd} measures the displacement of P from the equilibrium position defined in Fig. 1, while $d^{tp}_{P-Ni}/d^{tp}_{P-Pd}$ captures a displacement that involves the vertical axis of Fig. 1.

In Fig. 4 one can see the effect of the Si inclusion in the compound $Pd_{32}Ni_{64}P_{31}Si_1$ in a cell of 128. This compound has been chosen because it has the lowest proportion of Si. As a result, one can estimate the influence length of the inclusion. From Fig. 4 it is clear that such length is around 14 Å. This length is consistent with the idea of having at least a 1% or 2% of Si, since if we want to cover all the P atoms in the system inside non-intersecting 14 Å spheres centered in Si, the result turns out to be around ≈1.2%. For smaller Si concentrations, some P-based clusters are too far away to be affected, while too much Si leads to overlapping spheres in which Si based crystals can grow. (See Fig. 3.)

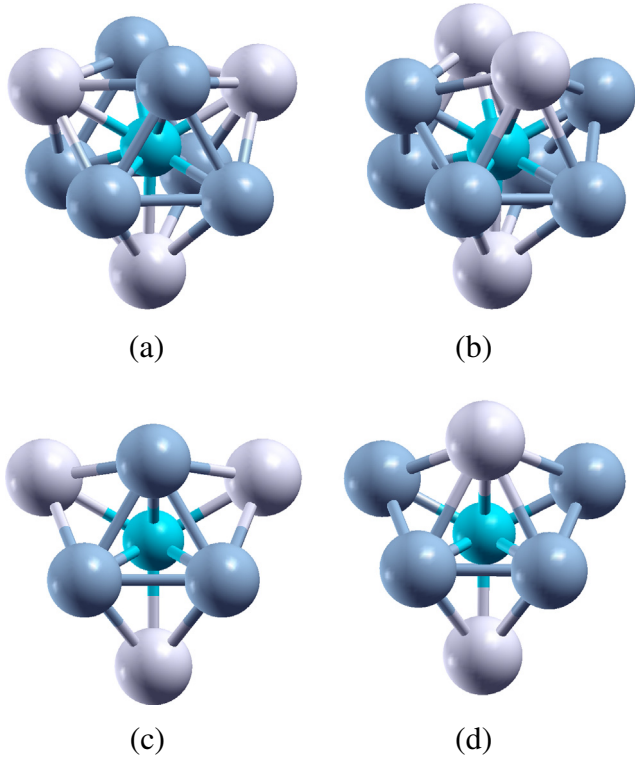

Fig. 3. Insets 3-a and 3-c correspond to the same PdNiSi crystalline cluster viewed in two different orientations around the Si atom. Insets 3-b and 3-d correspond to different views of the same cluster around the Si atom for the supercell $Pd_{32}Ni_{64}P_{31}Si_1$.

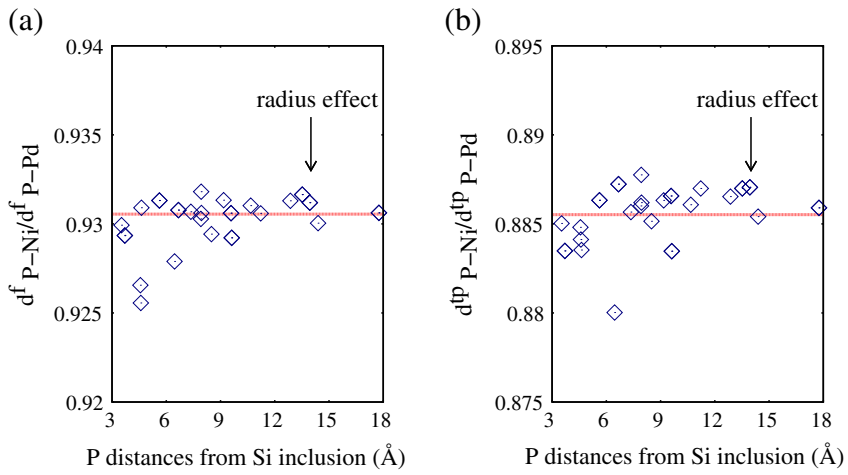

Fig. 4. Distances ratios of P from a Si inclusion in a cell of 128 atoms in the compound $Pd_{32}Ni_{64}P_{31}Si_1$. In inset 4-a, d^f_{P-Ni} and d^f_{P-Pd} are the distances from the central P to the Ni and Pd situated on the faces of the trigonal prisms. In inset 4-b, d^{tp}_{P-Ni} and d^{tp}_{P-Pd} are the distances from the central P to the Ni and Pd situated on the corners of the trigonal prisms, see Fig. 1. The arrow indicates the maximal radius of the perturbation.

This suggests an idea on how Si has an influence on the devitrification dynamics, which is a complex process of crystallite nucleation and phase separation [19–25]. This complex process can be represented by paths in a high-dimensional phase space [37–39]. Along these paths, the off-center P displacement has a knock-on effect (domino effect), with each successive off-center P displacement pushing the next off-center P displacement, and so on resulting in an internal stress transmission. Introducing a small amount of Si interrupts this process. The local pressure and strain induced by Si also can have an impact in the glass transition temperature through the vibrational properties of the glass by increasing its local connectivity [26,40–43].

3.2. Electronic properties

In Fig. 5 we present a comparison between the DOS of PdNiP and $PdNi_2P$. For PdNiP, the DOS is higher at the fermi energy (E_F) than for $PdNi_2P$. This suggests that $PdNi_2P$ crystal is more stable, as is also reflected in the cohesive energies, see Table 3. This fact is well supported by a recent study of atomic tomography of crystalline and amorphous Pd–Ni–P system [14]. It has been found that heterogeneous microcrystals were basically made of $PdNi_2P$, while glasses tended to be richer in Pd.

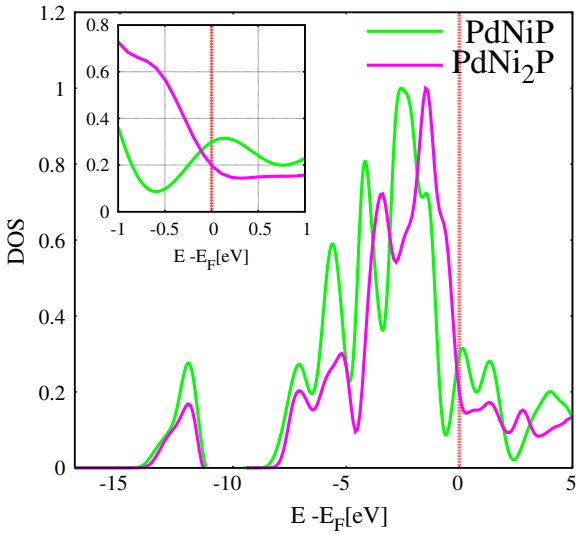

Fig. 5. Comparison of the electronic density of states for PdNiP and $PdNi_2P$ crystals. The Fermi energy is marked with a vertical red line and has been set to zero. (For interpretation of the references to color in this figure legend, the reader is referred to the web version of this article.)

From Figs. 5 to 9, we provide an overall picture of the substitution effects of P by Si in the electronic structure of the relaxed related crystals. There are two noticeable features,1) As seen in Figs. 5, 7 and 9, a small bump appears at −10 eV below the E_F when Si is added. At the same time, the bump around −15 eV decreases. Such effect is easily explained by looking at the band structure. In the partial DOS (pDOS) on each kind of atom, the bump at −15 eV is due to valence 3s states of P, while the bump at −10 eV is due to the Si 3s states, see for example cases PdNiP and PdNiSi pDOS of Figs. 6 and 8 respectively.

Also, from the partial DOS, an important feature that we found is that the *s* states in Si are much more hybridized with the *d* states of the transition metals (TM). This means that s states have a more important role in the bonding, as is reflected in the cohesion energy of the systems (see Table 3). The effect of Si is to increase the cohesion energy.

It is important to remark that the hybridized bands of *p* states of Si and P with the *d* bands of the TM are similar in energy, around −5 eV. The Si *p-d* hybridized orbitals tend to lie in a slightly higher energy, so the main reason for the increased cohesion is the hybridization of *s* orbitals of Si when compared with P.

2) For PdNiP, E_F falls near a peak, as seen in Fig. 7. In this compound, a few percentage substitution of Si tends to move E_F to the bottom of a nearby pseudogap, indicating a tendency for cluster stabilization. If P is completely replaced by Si, E_F lies very close to the bottom of a deep pseudogap, as seen in Fig. 7. On the other hand, for $PdNi_2Si$, the DOS is bigger at E_F in Fig. 7 and has less cohesion than in PdNiSi, as seen in Table 3.

For $Pd_{20}Ni_{60}P_{20}$ related systems, E_F is close to a plateau in the DOS. The inclusion of a small percentage of Si increases the tendency of E_F

Table 3
Cohesive energies for Pd–Ni–P, Pd–Ni–Si systems and the supercells with the Si inclusion in cells of 8, 16, 32, 64 and 128 atoms.

System	(eV/atom)	System	(eV/atom)
PdNiP	5.2636	PdNiSi	5.4270
$PdNi_2P$	5.4213	$PdNi_2Si$	5.4173
Si inclusion in variable cells			
$Pd_2Ni_4P_2$	5.4213	$Pd_2Ni_4P_1Si_1$	5.4219
$Pd_4Ni_4P_4$	5.4211	$Pd_4Ni_8P_3Si_1$	5.4221
$Pd_8Ni_{16}P_8$	5.4341	$Pd_4Ni_{16}P_7Si_1$	5.4345
$Pd_{16}Ni_{32}P_{16}$	5.4314	$Pd_{16}Ni_{32}P_{15}Si_1$	5.4324
$Pd_{328}Ni_{64}P_{32}$	5.4292	$Pd_{32}Ni_{64}P_{31}Si_1$	5.4293

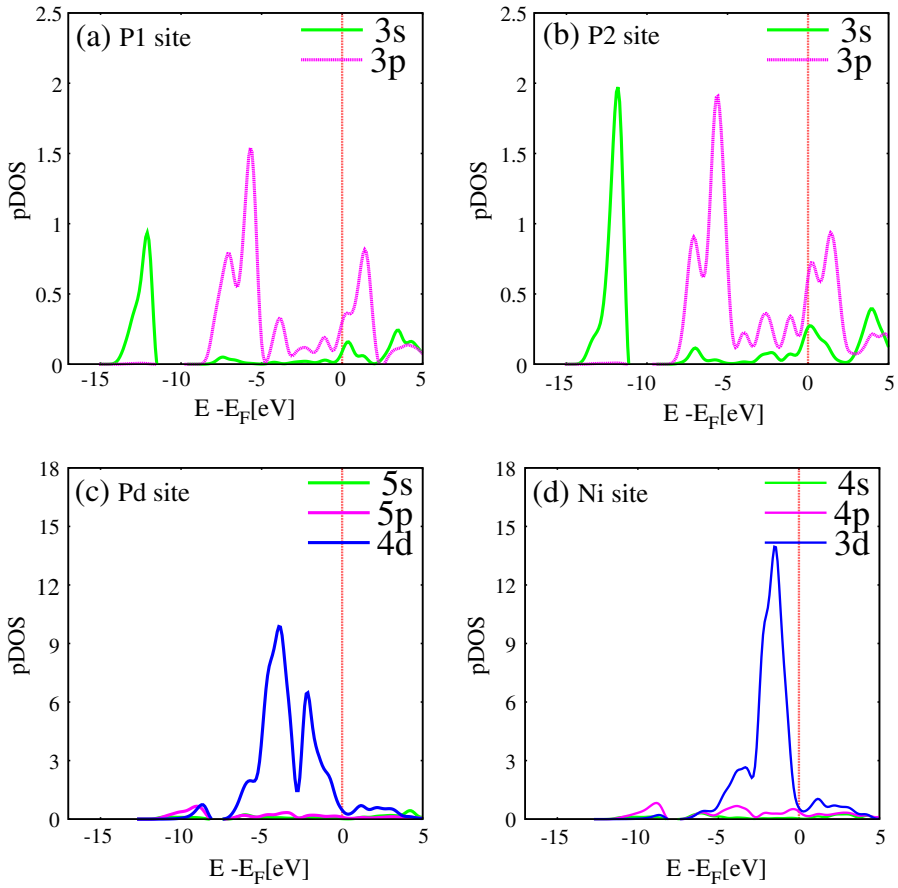

Fig. 6. Partial density of states at different local atomic environments for PdNiP after variable cell relax. The Fermi energy is marked with a vertical red line, and has been set to zero. (For interpretation of the references to color in this figure legend, the reader is referred to the web version of this article.)

to move near the minimum in all compounds. However, at equal percentages of Si and P, the DOS increases at E_F, a fact that may explain why too much Si is also bad for glass forming ability (GFA) in $PdNi_2P$.

The fact that DOS is a local maximum at E_F in PdNiP and has less cohesion when compared with $PdNi_2P$ needs to be contrasted with the opposite behavior of Si. A deep pseudogap appears at E_F for PdNiSi and the system has a higher cohesion than in $PdNi_2P$. Thus, Si favors Pd rich phases with a symmetric configuration of the transition metal at the faces of the trigonal prisms, while P favors Ni rich with an asymmetric configuration. This means that Si can enhance several competing crystals which eventually help to inhibit devitrification.

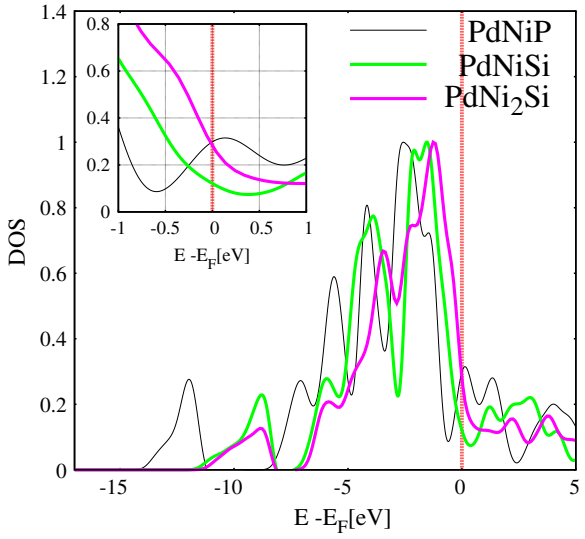

Fig. 7. Comparison of the electronic density of states for PdNiP, PdNiSi and $PdNi_2Si$ crystals. The Fermi energy is marked with a vertical red line, and has been set to zero. (For interpretation of the references to color in this figure legend, the reader is referred to the web version of this article.)

4. Conclusions

In conclusion, the structural and electronic effects of Si addition in Pd–Ni–P systems were analyzed. Under the assumption that Si replaces P inside the center of trigonal pyramids, we obtained that Si prefers clusters based on a rich Pd environment with a symmetric configuration of the transition metal at the faces, while P prefers a Ni rich environment with an asymmetric arrangement of the transition metals. Also, Si tends to be at the center of the clusters, while P presents a displacement towards some of the Ni atoms. As a result, in general the coordination of Si is higher than the one observed for P atoms. These observations help to understand why Si improves the GFA, since Si favors the formation of different competing crystalline phases. Furthermore, the inclusion of Si leads to a local expansion of the cluster, inducing a local pressure field around surrounding P clusters, which promotes disorder in the positions and coordination of the P-based clusters. The radius of influence of such "shoving effect" is around 14 Å, which explains in a rough way the experimental finding that a 1% or 2% of Si increases the glass forming ability.

The present work suggests that devitrification can be understood as complex cooperative phenomena, in which each successive off-center P displacement inside the basic cluster pushes the next off-center P displacement, favoring crystallization. It seems that a small amount of Si

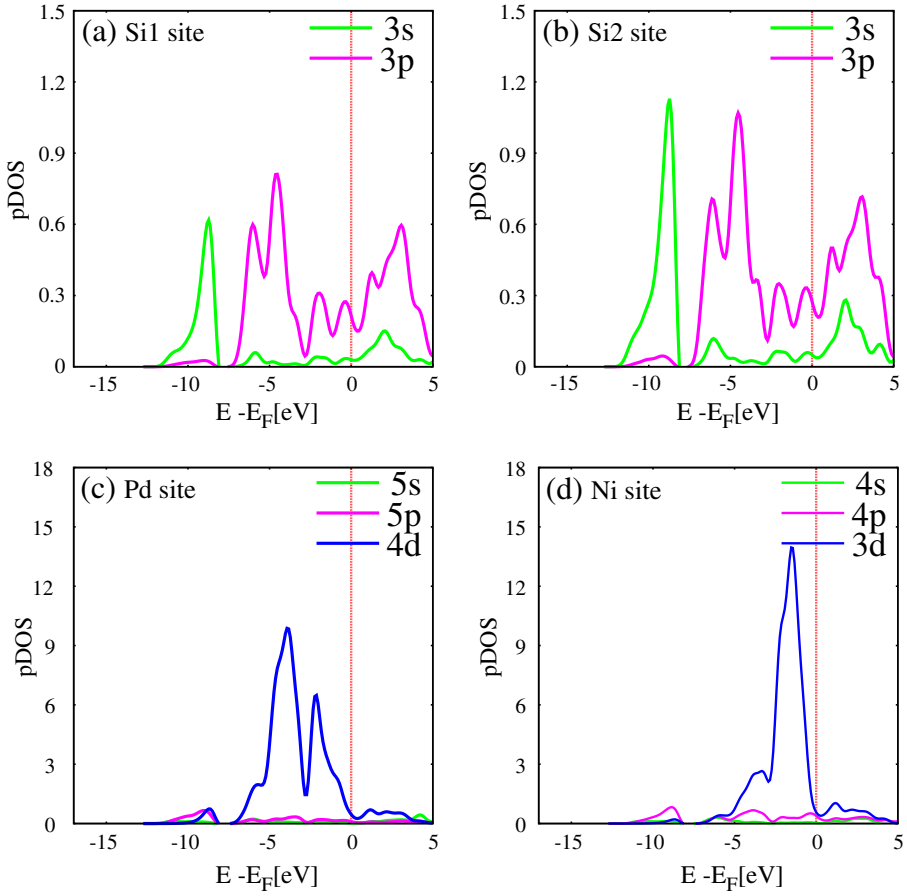

Fig. 8. Partial density of states at different local atomic environments for PdNiSi after variable cell relax. The Fermi energy is marked with a vertical red line, and has been set to zero. (For interpretation of the references to color in this figure legend, the reader is referred to the web version of this article.)

interrupts this cooperative phenomenon. The local pressure and increased rigidity of the lattice induced by Si can also have an impact in the glass transition temperature and rheology [26,40–43]. Some of these interesting questions will be the subject of future works.

Acknowledgment

We thank a lot J. C. Phillips for the enlightening discussions and for providing key bibliography. The authors thank DGTIC-UNAM. JARR acknowledges support from DGAPA-UNAM. This work was partially supported by the DGAPA project IN-102513. Calculations were made in the NES supercomputer of the DGTIC-UNAM.

References

[1] M.F. Ashby, A.L. Greer, Metallic glasses as structural materials, Scr. Mater. 54 (3) (2006) 321–326.
[2] W.H. Wang, C. Dong, C.H. Shek, Bulk metallic glasses, Mater. Sci. Eng. R. 44 (2004) 45–89.
[3] W. Klement, R.H. Willens, P. Duwez, Non-crystalline structure in solidified gold–silicon alloys, Nature 187 (1960) 869–870.
[4] H.S. Chen, Thermodynamic considerations on the formation and stability of metallic glasses, Acta Metall. 22 (12) (1974) 1505–1511.
[5] A.J. Drehman, A.L. Greer, D. Turnbul, Bulk formation of a metallic glass: $Pd_{40}Ni_{40}P_{20}$, Appl. Phys. Lett. 41 (8) (1982).
[6] H.W. Kui, Al L. Greer, D. Turnbull, Formation of bulk metallic glass by fluxing, Appl. Phys. Lett. 45 (1984) 615.
[7] Akihisa Inoue, Stabilization of metallic supercooled liquid and bulk amorphous alloys, Acta Mater. 48 (1) (2000) 279–306.
[8] Nobuyuki Nishiyama, Akihisa Inoue, Glass-forming ability of bulk $Pd_{40}Ni_{10}Cu_{30}P_{20}$ alloy, Mater. Trans. JIM 37 (10) (1996) 1531–1539.
[9] N. Nishiyama, A. Inoue, Glass-forming ability of PdCuNiP alloy with a low critical cooling rate of 0.067 k/s, Appl. Phys. Lett. 80 (2002) 568.
[10] David Turnbull, Under what conditions can a glass be formed? Contemp. Phys. 10 (5) (1969) 473–488.
[11] Z.P. Lu, C.T. Liu, Glass formation criterion for various glass-forming systems, Phys. Rev. Lett. 91 (11) (2003) 115505.
[12] A. Garcia Escorial, A.L. Greer, Surface crystallization of melt-spun $Pd_{40}Ni_{40}P_{20}$ glass, J. Mater. Sci. 22 (12) (1987) 4388–4394.
[13] Yi He, R.B. Schwarz, J.I. Archuleta, Bulk glass formation in the Pd–Ni–P system, Appl. Phys. Lett. 69 (13) (1996) 1861–1863.
[14] J.S. Yu, Y.Q. Zeng, T. Fujita, T. Hashizume, A. Inoue, T. Sakurai, M.W. Chen, On the effect of impurities in metallic glass formation, Appl. Phys. Lett. 96 (14) (2010) 141901.
[15] N. Chen, D.V. Louzguine-Luzgin, G.Q. Xie, T. Wada, A. Inoue, Influence of minor Si addition on the glass-forming ability and mechanical properties of $Pd_{40}Ni_{40}P_{20}$ alloy, Acta Mater. 57 (9) (2009) 2775–2780.
[16] Y.Q. Zeng, A. Inoue, N. Nishiyama, M.W. Chen, Ni-rich Ni–Pd–P bulk metallic glasses with significantly improved glass-forming ability and mechanical properties by Si addition, Intermetallics 18 (9) (2010) 1790–1793.
[17] I.A. Figueroa, H.A. Davies, I. Todd, High glass formability for Cu–Hf–Ti alloys with small additions of Y and Si, Philos. Mag. 89 (27) (2009) 2355–2368.
[18] Tsunehiro Takeuchi, Daisuke Fukamaki, Hidetoshi Miyazaki, Kazuo Soda, Masashi Hasegawa, Hirokazu Sato, Uichiro Mizutani, Takahiro Ito, Shinichi Kimura, Electronic structure and stability of the Pd–Ni–P bulk metallic glass, Mater. Trans. 48 (6) (2007) 1292–1298.
[19] J.C. Phillips, Stretched exponential relaxation in molecular and electronic glasses, Rep. Prog. Phys. 59 (9) (1996) 1133.
[20] J.C. Phillips, Slow dynamics in glasses: a comparison between theory and experiment, Phys. Rev. B 73 (Mar 2006) 104206.
[21] J.C. Phillips, Microscopic aspects of stretched exponential relaxation (ser) in homogeneous molecular and network glasses and polymers, J. Non-Cryst. Solids 357 (22–23) (2011) 3853–3865.
[22] Roger C. Welch, et al., Dynamics of glass relaxation at room temperature, Phys. Rev. Lett. 110 (Jun 2013) 265901.
[23] John C. Mauro, Statistics of modifier distributions in mixed network glasses, J. Chem. Phys. 138 (12) (2013).
[24] John C. Mauro, Morten M. Smedskjaer, Unified physics of stretched exponential relaxation and weibull fracture statistics, Phys. A 391 (23) (2012) 6121–6127.
[25] G.G. Naumis, J.C. Phillips, Bifurcation of stretched exponential relaxation in microscopically homogeneous glasses, J. Non-Cryst. Solids 358 (5) (2012) 893–897.
[26] Hugo M. Flores-Ruiz, Gerardo G. Naumis, J.C. Phillips, Heating through the glass transition: a rigidity approach to the boson peak, Phys. Rev. B 82 (Dec 2010) 214201.

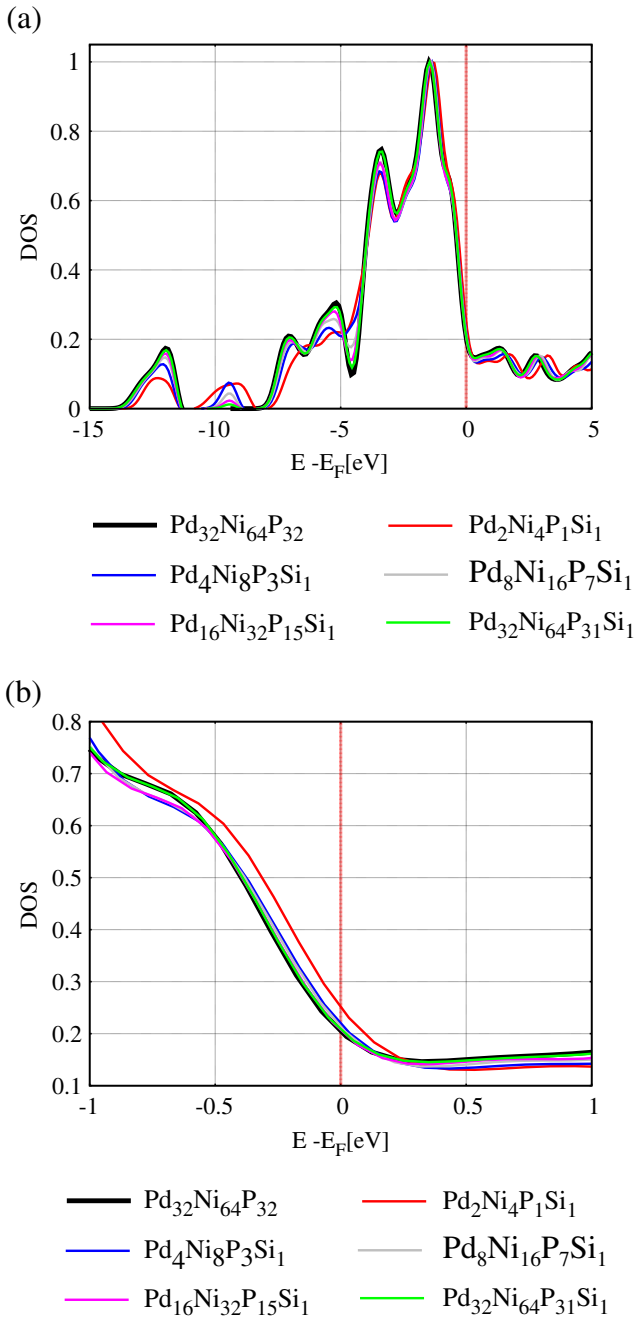

Fig. 9. The electronic density of states for $PdNi_2(P_{1-x}Si)$. Inset 9-b is a blow-up around E_F of the inset 9-a.

[27] Pierre Villars, Lauriston D. Calvert, Pearson's Handbook of Crystallographic Data for Intermetallic Phases, 2, American Society for Metals Park, OH, 1985.
[28] M. Vennstrom, J. Howing, T. Gustafsson, Y. Andersson, The crystal structures of $PdNi_2P$ and $Pd_8Ni_{31}P_{16}$, J. Solid State Chem. 177 (4–5) (2004) 1449–1455.
[29] Paolo Giannozzi, Stefano Baroni, Nicola Bonini, Matteo Calandra, Roberto Car, Carlo Cavazzoni, Davide Ceresoli, Guido L. Chiarotti, Matteo Cococcioni, Ismaila Dabo, Andrea Dal Corso, Stefano de Gironcoli, Stefano Fabris, Guido Fratesi, Ralph Gebauer, Uwe Gerstmann, Christos Gougoussis, Anton Kokalj, Michele Lazzeri, Layla Martin-Samos, Nicola Marzari, Francesco Mauri, Riccardo Mazzarello, Stefano Paolini, Alfredo Pasquarello, Lorenzo Paulatto, Carlo Sbraccia, Sandro Scandolo, Gabriele Sclauzero, Ari P. Seitsonen, Alexander Smogunov, Paolo Umari, Renata M. Wentzcovitch, Quantum espresso: a modular and open-source software project for quantum simulations of materials, J. Phys. Condens. Matter 21 (39) (2009) 395502.
[30] GNU General Public License, Free Software Foundation, GNU Project, 1991.
[31] David Vanderbilt, Soft self-consistent pseudopotentials in a generalized eigenvalue formalism, Phys. Rev. B 41 (Apr 1990) 7892–7895.
[32] Andrew M. Rappe, Karin M. Rabe, Efthimios Kaxiras, J.D. Joannopoulos, Optimized pseudopotentials, Phys. Rev. B 41 (Jan 1990) 1227–1230.
[33] John P. Perdew, J.A. Chevary, S.H. Vosko, Koblar A. Jackson, Mark R. Pederson, D.J. Singh, Carlos Fiolhais, Atoms, molecules, solids, and surfaces: applications of the generalized gradient approximation for exchange and correlation, Phys. Rev. B 46 (Sep 1992) 6671–6687.
[34] John P. Perdew, Kieron Burke, Matthias Ernzerhof, Generalized gradient approximation made simple, Phys. Rev. Lett. 77 (Oct 1996) 3865–3868.
[35] Jeppe C. Dyre, Niels Boye Olsen, Tage Christensen, Local elastic expansion model for viscous-flow activation energies of glass-forming molecular liquids, Phys. Rev. B 53 (Feb 1996) 2171–2174.
[36] Jeppe C. Dyre, Source of non-arrhenius average relaxation time in glass-forming liquids, J. Non-Cryst. Solids 235 (1998) 142–149.
[37] Richard Kerner, Gerardo G. Naumis, Stochastic matrix description of the glass transition, J. Phys. Condens. Matter 12 (8) (2000) 1641.
[38] Gerardo G. Naumis, Richard Kerner, Stochastic matrix description of glass transition in ternary chalcogenide systems, J. Non-Cryst. Solids 231 (1998) 111–119.
[39] A. Huerta, G.G. Naumis, Relationship between glass transition and rigidity in a binary associative fluid, Phys. Lett. A 299 (2002) 660–665.
[40] Gerardo G. Naumis, Contribution of floppy modes to the heat capacity jump and fragility in chalcogenide glasses, Phys. Rev. B 61 (Apr 2000) R9205–R9208.
[41] Gerardo G. Naumis, Hugo M. Flores-Ruiz, Low-frequency vibrational mode anomalies and glass transition: thermal stability, phonon scattering, and pressure effects, Phys. Rev. B 78 (Sep 2008) 094203.
[42] Gerardo G. Naumis, Glass transition phenomenology and flexibility: an approach using the energy landscape formalism, J. Non-Cryst. Solids 352 (42) (2006) 4865–4870.
[43] Gerardo G. Naumis, Variation of the glass transition temperature with rigidity and chemical composition, Phys. Rev. B 73 (May 2006) 172202.